

# Log-Poisson Non-Gaussianity of $\text{Ly}\alpha$ Transmitted Flux Fluctuations at High Redshift

Yi Lu<sup>1\*</sup>, Weishan Zhu<sup>2,3</sup>, Yaoquan Chu<sup>1</sup>, Long-long Feng<sup>3</sup>, Li-Zhi Fang<sup>2</sup>

<sup>1</sup>*Center for Astrophysics, University of Science and Technology of China, Hefei, Anhui 230026, China*

<sup>2</sup>*Department of Physics, University of Arizona, Tucson, AZ 85721*

<sup>3</sup>*Purple Mountain Observatory, Nanjing, 210008, China*

24 October 2018

## ABSTRACT

We investigate the non-Gaussian features of the IGM at redshift  $z \sim 5 - 6$  using  $\text{Ly}\alpha$  transmitted flux of quasar absorption spectra and cosmological hydrodynamic simulation of the concordance  $\Lambda$ CDM universe. We show that the neutral hydrogen mass density field and  $\text{Ly}\alpha$  transmitted flux fluctuations possess all the non-Gaussian features predicted by the log-Poisson hierarchy, which depends only on two dimensionless parameters  $\beta$  and  $\gamma$ , describing, respectively, the intermittence and singularity of the random fields. We find that the non-Gaussianity of the  $\text{Ly}\alpha$  transmitted flux of quasars from  $z = 4.9$  to  $z = 6.3$  can be well reconstructed by the hydrodynamical simulation samples. Although the Gunn-Peterson optical depth and its variance underwent a significant evolution in the redshift range of  $5 - 6$ , the intermittency measured by  $\beta$  is almost redshift-independent in this range. More interesting, the intermittency of quasar's absorption spectra on physical scales  $0.1 - 1 \text{ h}^{-1}\text{Mpc}$  in redshift  $5 - 6$  are found to be about the same as that on physical scales  $1 - 10 \text{ h}^{-1}\text{Mpc}$  at redshifts  $2 - 4$ . Considering the Jeans length is less than  $0.1 \text{ h}^{-1}\text{Mpc}$  at  $z \sim 5$ , and  $1 \text{ h}^{-1}\text{Mpc}$  at  $z \sim 2$ , these results imply that the nonlinear evolution in high and low redshifts will lead the cosmic baryon fluid to a state similar to fully developed turbulence. The log-Poisson high order behavior of current high redshift data of quasar's spectrum can be explained by uniform UV background in the redshift range considered. We also studied the log-Poisson non-Gaussianity by considering inhomogeneous background. With several simplified models of inhomogeneous background, we found the effect of the inhomogeneous background on the log-Poisson non-Gaussianity is not larger than 1-sigma.

**Key words:** cosmology: theory - large-scale structure of universe

## 1 INTRODUCTION

The cosmic density and velocity fields of the intergalactic medium (IGM) at low redshifts are highly non-Gaussian, while the temperature fluctuations of the cosmic microwave background radiation basically are Gaussian or at most weakly non-Gaussian. Thus, the non-Gaussian features of the IGM at low redshifts should mainly result from nonlinear dynamical processes. A well knowledge of these non-Gaussian features and their development history can fundamentally improve our understanding of the formation and evolution of the structures in the universe. For instance, the lognormal clustering model of the IGM (Bi, 1993; Bi & Davidson 1997; Liu et al 2006; Feng et al 2008) can explain well all the basic properties of the  $\text{Ly}\alpha$  forests of quasar's absorption spectrum at various redshifts. However, high order statistics do reveal the deviation of

observation from the lognormal model (Jamkhedkar et al. 2003; Lu et al 2009).

The aim of this paper is to study the non-Gaussian features of  $\text{Ly}\alpha$  transmission flux of quasar spectrum at high redshift. The non-Gaussianities of high redshift  $\text{Ly}\alpha$  transmission flux have been studied by various statistics, including the probability distribution function (PDF) of the flux (Fan et al. 2002; Becker et al. 2007), the distribution of the size of dark gaps (Songaila & Cowie 2002; Fan et al 2006), the largest peak width distribution (Gallerani et al 2007) and the distributions of the width of leaks (Liu et al 2007; Feng et al 2008). Most of these statistics are designed based on the following observation facts: the high redshift quasar absorption spectra consist of complete absorption troughs separated by the spikes of transmitted flux. Obviously, these statistics are not suitable for comparing the non-Gaussian features at high redshift and low redshift, as the absorption spectra of low redshift quasars consist of  $\text{Ly}\alpha$  forests and do not contain Gunn-Peterson troughs. Our focus is on the log-Poisson non-Gaussianity, which are characterized by

\* E-mail: lulu@mail.ustc.edu.cn

two dimensionless parameters that are available for both high and low redshift samples. Therefore, it can be a useful tool to study the redshift evolution of non-Gaussianity.

More important, log-Poisson hierarchy is directly related to the dynamics of cosmic baryon fluid. With the cosmological hydrodynamical simulation of the concordance  $\Lambda$ CDM model, it has been shown that, in the scale range from the onset of nonlinear evolution to the scale of dissipation, the velocity fields of cosmic baryon fluid at low redshift are extremely well described by the She-Leveque's scaling formula (He et al 2006), which was inferred from the log-Poisson hierarchical cascade (Dubrulle 1994; She & Waymire 1995; Benzi et al. 1996). The non-Gaussian behavior of the mass density field of the baryon fluid also can be well described by log-Poisson processes (Liu & Fang 2008). Recently, high order statistics of observed high resolution and high S/N Ly $\alpha$  absorption spectra of quasars at redshift  $z \sim 2-3$  are found to be well consistent with the non-Gaussian features predicted by the log-Poisson hierarchy (Lu et al 2009). It would be worth to study whether the scenario of self-similar log-Poisson hierarchical cascade is still hold at high redshifts. Whether the log-Poisson non-Gaussianity experience a strong evolution in the redshift range 5 - 6? Can we explain the log-Poisson non-Gaussianity and its redshift dependence with the concordance  $\Lambda$ CDM model?

A possible application of the non-Gaussianity of neutral hydrogen distribution is to constrain the fluctuations of hydrogen-ionizing radiation background field. Considering the inhomogeneity of UV background might be a source of the non-Gaussianity of ionized and neutral hydrogen, the non-Gaussianity of Ly $\alpha$  transmitted flux would shed light on the evolution of UV background. The inhomogeneity of UV background at lower redshifts are negligible and a uniform ionizing background is an reasonable approximation. The situation becomes more complex and debatable when  $z > 5$  (Fan et al. 2002; Wyithe & Loeb 2005; Liu, et al. 2006; Fan et al. 2006; Liu et al. 2007; Mesinger & Furlanetto, 2009; Furlanetto & Mesinger 2009). Therefore, it is also worth to study the effect of non-uniform UV background on the log-Poisson high order behavior at high redshifts.

This paper is organized as follows. §2 gives the theoretical background. §3 presents the log-Poisson hierarchy of Ly $\alpha$  transmitted flux fluctuations of observed samples of high redshift quasar absorption spectra. In §4, we describe the method used for producing simulation samples, and show the log-Poisson non-Gaussianity of the neutral hydrogen component of cosmic baryon fluid. §5 compares the log-Poisson non-Gaussianities of observed data with simulation samples of Ly $\alpha$  transmitted flux. The effect of non-uniform UV background on non-Gaussianity is also studied in §5. Finally, conclusion and discussion are given in §6.

## 2 THEORETICAL BACKGROUND

### 2.1 Hierarchical clustering

It has been recognized for a long time that the clustering process of cosmic matter probably is hierarchical (Peebles 1980). That is, the nonlinear dynamics of large scale structure formation can be characterized by the merging of holes from smaller to larger scales. An early model of hierarchical clustering assumes that the correlation functions of the density field satisfy a linked-pair relation,  $\zeta_n = Q_n \zeta_2^{n-1}$  (White, 1979), where  $\zeta_n$  is the  $n$ th irreducible correlation function with variable  $\delta\rho(\mathbf{x}) = \rho(\mathbf{x}) - \bar{\rho}$ , where  $\rho(\mathbf{x})$  and  $\bar{\rho}$  are, respectively, the cosmic mass density field and its mean. However, observation samples of transmitted flux of Ly $\alpha$  forest do not

support the linked-pair relation if the coefficients  $Q_n$  are assumed to be constants (e.g. Feng et al. 2001).

The hierarchical merging has also been modeled by an additive cascade rule (Cole and Kaiser, 1988). The basic step of the cascade rule is to assume that the a cell of mass  $M$  and spatial scale  $x$  will evolve into two cells, 1 and 2 with mass  $M_1 = M + \delta m$  and  $M_2 = M - \delta m$ , on scale  $x/2$ , where  $\delta m$  is a Gaussian random variable. However, central limit theorem shows that the field produced by an additive cascade process should be Gaussian. It cannot explain the non-Gaussian features of Ly $\alpha$  transmitted flux (Pando et al. 1998). Moreover, this cascade needs a "very small initial units" (Peacock, 1999) as the first generation halo of the hierarchy, of which the mass is non-zero. This "initial units" is not compatible with hydrodynamic equations with continuous variables.

A proper model of the the hierarchical clustering should be randomly multiplicative, and infinitely divisible. For a randomly multiplicative cascade, the mass  $m_n$  in a cell at step  $n$  is related to step  $n-1$  by  $m_n = (1 \pm \delta)m_{n-1}$ , where  $\delta$  is a random variable. Non-Gaussian features can be formed through randomly multiplicative cascade processes, even if the original field is Gaussian. The infinite divisibility means that there is no finite "initial units" in the hierarchical merging. The "initial units" of the merging process can be infinitesimal.

The log-Poisson hierarchy has all these desired properties. More important, the log-Poisson hierarchy actually was inferred from the invariance and symmetry of the Navier-Stokes equations and works well in explaining the high order behavior of fully developed turbulence (Dubrulle, 1994; She & Waymire 1995; Leveque & She 1997).

### 2.2 Log-Poisson hierarchy

To measure the non-Gaussianity caused by log-Poisson hierarchy, it is better to use the variable  $\delta\rho_r = \rho(\mathbf{x} + \mathbf{r}) - \rho(\mathbf{x})$ ,  $r = |\mathbf{r}|$ , but not  $\rho(\mathbf{x} + \mathbf{r}) - \bar{\rho}$ . For a statistically isotropic and homogeneous random field, one can just consider  $|\delta\rho_r|$ , as the distribution of positive and negative  $\delta\rho_r$  is statistically symmetric. The basic statistical quantity is the structure function defined by

$$S_p(r) \equiv \langle |\delta\rho_r|^p \rangle, \quad (1)$$

where  $p$  is the order of statistics, and the average  $\langle \dots \rangle$  is taken over the ensemble of density fields. The second-order structure function  $S_2 = \langle |\delta\rho_r|^2 \rangle$  as a function of  $r$  (scale) is actually the power spectrum of the mass density field (Fang & Feng 2000).

In scale-free range, the structure function should be a function of power law of  $r$  as

$$S_p(r) \propto r^{\xi(p)}, \quad (2)$$

where  $\xi(p)$  is referred to intermittent exponent. For a Gaussian field,  $\xi(p)$  is a linear function of  $p$ , but for a intermittent field, function  $\xi(p)$  is nonlinear.

The log-Poisson hierarchy assumes that, in the scale-free range, the variables  $\delta\rho_r$  on different scales  $r$  are related to each other by a statistically hierarchical relation as (Dubrulle 1994; She & Waymire 1995)

$$\delta\rho_{r_2} = W_{r_1 r_2} \delta\rho_{r_1}. \quad (3)$$

The factor  $W_{r_1 r_2}$  is a function of the ratio  $r_1/r_2$  given by

$$W_{r_1 r_2} = \beta^m (r_1/r_2)^\gamma, \quad (4)$$

which describes how the fluctuation  $\delta\rho_{r_1}$  on the larger scale  $r_1$  relates to fluctuations  $\delta\rho_{r_2}$  on the smaller scale  $r_2$ . In eq.(4),  $m$  is a Poisson random variable with the PDF

$$P(m) = \exp(-\lambda_{r_1 r_2}) \lambda_{r_1 r_2}^m / m!. \quad (5)$$

The random variable  $m$  can be considered as the steps of the evolution from  $\delta\rho_{r_1}$  to  $\delta\rho_{r_2}$ . To ensure the normalization  $\langle W_{r_1 r_2} \rangle = 1$ , where the average  $\langle \dots \rangle$  is over  $m$ , the mean  $\lambda_{r_1 r_2}$  of the Poisson distribution is then

$$\lambda_{r_1 r_2} = \gamma [\ln(r_1/r_2)] / (1 - \beta). \quad (6)$$

The log-Poisson hierarchy contains both the spatial size and amplitude of the density fluctuations. This point is different from other hierarchical models, which consider only the size of hierarchical units.

The log-Poisson hierarchy given by eq.(3) depends only on the ratio  $r_1/r_2$ , which is obviously scale invariant. The hierarchy is determined by two dimensionless positive parameters:  $\beta$  and  $\gamma$ , describing, respectively, the intermittence and singularity of the random fields. Equation (3) relates  $\delta\rho_r$  on different scales by multiplying a random factor  $W$ , which generally yields a non-Gaussian field even if the field originally is Gaussian (Pando et al. 1998).

The cascade from scale  $r_1$  to  $r_2$ , and then to  $r_3$  is identical to the cascade from  $r_1$  to  $r_3$ . It is because  $W_{r_1 r_3} = W_{r_1 r_2} W_{r_2 r_3} = \beta^N (r_1/r_3)^\gamma$ , where  $N$  is again a Poisson random variable with  $\lambda_{r_1 r_3} = \lambda_{r_1 r_2} + \lambda_{r_2 r_3} = \gamma [\ln(r_1/r_3)] / (1 - \beta)$ . The log-Poisson hierarchy removes an arbitrariness in defining the steps of cascade from  $r_1$  to  $r_2$  or  $r_2$  to  $r_3$ . Therefore, the log-Poisson hierarchy, suggested by eq.(3), is discrete in terms of the discrete random number  $m$ . However, the scale  $r$  is infinitely divisible. Namely, there is no lower limit on the difference  $r_1 - r_2$ . It can be infinitesimal, and the hierarchical process is of infinite divisibility. With the log-Poisson model eqs.(3)-(6), one can show that the intermittent exponent  $\xi(p)$  is given by (Liu & Fang 2008)

$$\xi(p) = -\gamma [p - (1 - \beta^p) / (1 - \beta)]. \quad (7)$$

This is actually the SL scaling formula (She & Leveque 1994).

From eq.(7), the power spectrum  $S_2(r) = \text{const}$  is flat, or called white. However, the power spectrum of the initial Gaussian field of the cosmic matter generally is not white, but colored with power-law  $S_2(r) \propto r^{-2\alpha}$ . In this case, we should adjust the log-Poisson hierarchy eq.(3) by replacing  $\delta\rho_{r_1}$  and  $\delta\rho_{r_2}$  with  $r_1^\alpha \delta\rho_{r_1}$  and  $r_2^\alpha \delta\rho_{r_2}$  respectively. The intermittent exponent  $\xi(p)$  is

$$\xi(p) = -\alpha p - \gamma [p - (1 - \beta^p) / (1 - \beta)]. \quad (8)$$

When parameter  $\alpha = 0$ , eq.(8) will simplify to eq.(7). The non-Gaussian features of the field described by the log-Poisson hierarchical clustering have been given in Liu & Fang (2008) and Lu et al (2009).

### 3 LOG-POISSON NON-GAUSSIANITY OF OBSERVED SAMPLES

#### 3.1 Observed data

Observational data used here consists of the spectra of 19 QSOs with redshifts from  $z = 5.74$  to  $6.42$  that compiled in Fan et al. (2006). The data have resolution of  $R \sim 3000 - 4000$  and are re-binned to a resolution  $R = 2600$ . The observed flux,  $f_{\text{obs}}$ , is normalized with a power-law continuum  $f_{\text{con}} \propto \nu^{-0.5}$ . The noise and continuum uncertainty of transmitted flux  $\mathbb{F} \equiv f_{\text{obs}}/f_{\text{con}}$  is in

the level of  $0.018 \pm 0.012$  in the range  $z \leq 5.7$ , and  $0.014 \pm 0.008$  in the range  $z > 5.7$  (Liu et al. 2007). For more details, we refer to Fan et al. (2006). Wavelength of the data covers roughly the rest-frame wavelength from  $900$  to  $1350 \text{ \AA}$ . To avoid the mixing of Ly $\beta$  absorption and the proximity effect, only pixels have the rest frame wavelength  $> 1040 \text{ \AA}$  and below the maximum Ly $\alpha$  are used.

In our analysis below, we use only the Ly $\alpha$  transmitted flux in the redshift range from  $4.7$  to  $6.3$ . There actually are 12 quasars available in the range  $z > 5.9$  and reduce further to 4 in  $6.1 < z < 6.3$ . We divide the redshift range from  $4.9$  to  $6.3$  into 7 bins by  $4.9 + n \times 0.20 < z < 4.9 + (n+1) \times 0.20$  where  $n = 0, 1, \dots, 6$ . More specifically, the redshift size of each bin is  $\Delta z = 0.20$ . As a comparison, we also use sample in the redshift range from  $4.7$  to  $6.2$ , and divide it into 10 bins by  $4.7 + n \times 0.15 < z < 4.7 + (n+1) \times 0.15$  where  $n = 0, 1, \dots, 9$ ; each bin has a size of  $\Delta z = 0.15$ . All the transmission flux pixels in a given redshift bin form an ensemble. The numbers of pixels in different ensemble are not uniform.

In order to compare with observation at moderate redshift we also analyze the high resolution and high signal to noise ratio Ly $\alpha$  absorption spectra of 28 Keck High Resolution (HIRES) QSO (Kirkman & Tytler 1997). It is the same as that used in Lu et al (2009). The details of the data set and its reduction have been described in Jamkhedkar et al. (2002, 2003).

With these samples we calculate the optical depth  $\tau(z) = -\ln \mathbb{F}(z)$ , and the fluctuation of the optical depth  $\delta\tau_r = \tau(x+r) - \tau(x)$ , where the spatial coordinates  $x$  and  $r$  are in physical scale. Since the variable  $\delta\tau_r$  is given by difference between  $\tau(x+r)$  and  $\tau(x)$ ,  $\delta\tau_r$  is independent of fluctuations of  $\tau(x)$  on scales larger than  $r$ . Therefore, the variable  $\delta\tau_r$  actually is insensitive to the continuum used in the data reduction (Jamkhedkar et al. 2001).

As has been shown in Lu et al (2009), the variable  $\delta\tau_r$  is approximately a measurement of the density fluctuation  $\rho_r$ . We can then study the log-Poisson non-Gaussianity with variable  $\delta\tau_r$ . For instance, the structure function with the variable  $\delta\tau_r$  is defined now by

$$S_p(r) \equiv \langle |\delta\tau_r|^p \rangle. \quad (9)$$

To treat the unwanted data, including low S/N and bad pixels, we use the algorithm of wavelet denoising by threshold (Donoho 1995, Jamkhedkar, et. al. 2003). This method is effective for pixelated data. First, we calculate the wavelet scaling function coefficients (SFCs) of both transmission flux field  $\mathbb{F}(x)$  and noise field  $n(x)$  with

$$\epsilon_{jl}^{\mathbb{F}} = \int \mathbb{F}(x) \phi_{j,l}(x) dx, \quad \epsilon_{jl}^N = \int n(x) \phi_{j,l}(x) dx. \quad (10)$$

where  $\phi_{j,l}(x)$  is the scaling function of wavelet on scale  $j$  and at position  $l$ . We then identify unwanted mode  $(j, l)$  by using the threshold condition

$$|\epsilon_{jl}^{\mathbb{F}} / \epsilon_{jl}^N| < f. \quad (11)$$

This condition flags all modes with S/N less than  $f$ . We skip all the flagged modes when doing statistics. To reduce the boundary effect of unwanted chunks, we also flag two models around an unwanted model. With this method, no rejoining and smoothing of the data are needed. The threshold  $f$  is given by the same way as Jamkhedkar et al (2003) and Lu et al (2009).

A typical statistical quantity of log-Poisson non-Gaussianity is

$$F_p(r) \equiv S_{p+1}(r) / S_p(r). \quad (12)$$

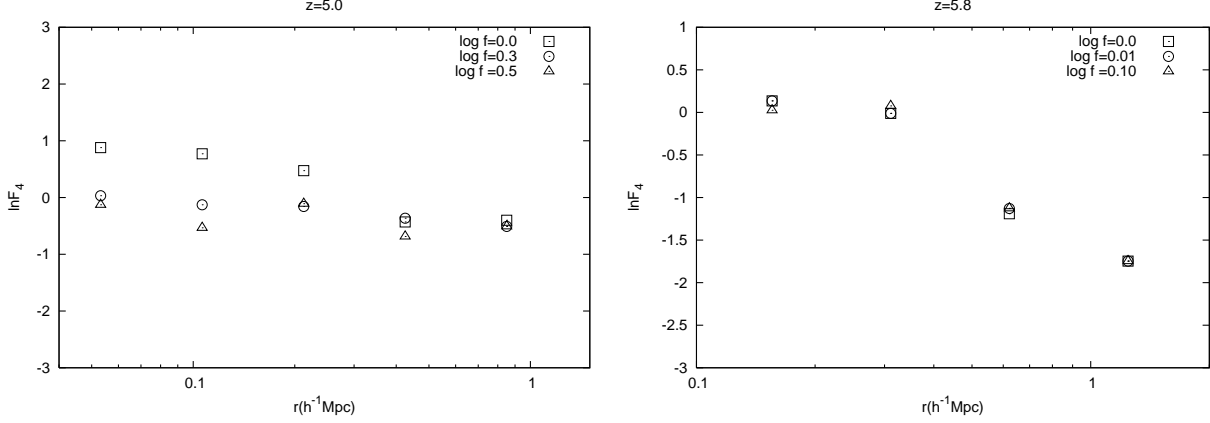


**Figure 1.**  $F_4(r)$  given by observed sample of the Ly $\alpha$  transmitted flux at redshift ranges  $4.9 < z < 5.1$  (left), and  $5.7 < z < 5.9$  (right).

We test the effect of noise on  $F_4(r) \equiv S_5(r)/S_4(r)$ . We calculate  $F_4(r)$  for data sets given by different threshold  $f$ . The  $f$ -dependence of  $F_4(r)$  is shown in Figure 1. For the data set at  $4.9 < z < 5.1$ , the values of  $F_4(r)$  are  $f$ -independent when  $\log f \geq 0.3$ . In other words, the statistical results are stable with respect to threshold  $f \simeq 2$ . We will use only data with S/N larger than 2. This threshold is larger than the error level given by Fan et al (2006). For sample set of  $5.7 < z < 5.9$  (right panel of Figure 1),  $F_4(x)$  are very weakly dependent on  $\log f$ . It is because, in the redshift range  $z > 5.7$ , the high order statistics  $F_4(x)$  are dominated by modes with high  $\delta\tau_r$ , and therefore, it is insensitive to dropping modes with low  $\delta\tau_r$ . However, the fewer the modes, the larger the variance of Poisson process. Therefore, we should consider the variance of Poisson process in our statistics.

### 3.2 Redshift dependence of parameter $\beta$

We first study the  $\beta$ -hierarchy predicted by the log-Poisson hierarchy. It reads (Liu & Fang, 2008)

$$\ln F_{p+1}(r)/F_3(r) = \beta \ln F_p(r)/F_2(r). \quad (13)$$

Eq.(13) requires that for *all*  $r$  and  $p$ ,  $\ln[F_{p+1}(r)/F_3(r)]$  vs.  $\ln[F_p(r)/F_2(r)]$  should be on a straight line with slope  $\beta$ , which is called  $\beta$ -hierarchy. Eq.(13) does not contain parameters  $\gamma$  and  $\alpha$ . Figure 2 presents the  $\beta$ -hierarchy of observed transmitted flux in 4 redshift ranges  $z = 5.0, 5.4, 5.8$  and  $6.2$ . The statistical quantity  $F_{p+1}(r)$  are given by all available observed data, of which the physical scale  $r$  covers the range from  $\sim 0.1$  to  $1.5 \text{ h}^{-1} \text{ Mpc}$ , and the order parameter  $p$  increases from 1 to 2.5. All the distributions of  $F_{p+1}(r)/F_3(r)$  vs.  $F_p(r)/F_2(r)$  in Figure 2 can be well fitted with a straight line. It shows that the Ly $\alpha$  transmitted flux of real observation at high redshifts still satisfy the  $\beta$ -hierarchy and indicates that the log-Poisson non-Gaussian features are significant in the considered redshift range.

From the  $\beta$ -hierarchy straight line, we calculate the parameter  $\beta$  in redshift ranges from  $z = 5.0$  to  $6.2$ . Figure 3(a) presents the mean of  $\beta$  in each redshift bin. The error bars are given by the variance of Poisson process, which generally are large than the variance of  $\beta$  in the given redshift bin. Figure 3(a) shows that the redshift evolution of  $\beta$  is rather weak in the range from  $z = 5$  to  $6$ . We also calculate the redshift-dependence of  $\beta$  with the same data,

but the size of redshift bin is taken to be  $\Delta z = 0.15$ . The result is also plotted in Figure 3(a), which shows the same redshift dependence as that of  $\Delta z = 0.20$ . Therefore, the weak redshift-evolution of parameter  $\beta$  does not affected by  $\Delta z$ . From now on, we will only give results with  $\Delta z = 0.20$ .

Figure 3(b) plots the redshift dependence of  $\beta$  for the Keck HIRES quasars spectra sample. The error bars are given by the maximum and minimum in each redshift interval. Comparing Figure 3(a) and (b), we can conclude that the non-Gaussian parameter  $\beta$  evolves weakly from redshift 2 to 6. It should be pointed out that the physical scale  $r$  in Figure 3(a) (high redshift sample) is actually smaller than that of Figure 3(b) (low redshift sample). Figure 3 reveals that the  $\beta$  non-Gaussianity on a small scale at high redshift are about equal to that on a large scale at low redshift. This result indicates that the turbulence state on scales  $0.1 - 1 \text{ h}^{-1} \text{ Mpc}$  at redshift  $z \sim 5$  would be the same as that on scales  $1 - 10 \text{ h}^{-1} \text{ Mpc}$  at redshift  $\sim 2$ . This is consist with the fact that the Jeans length at  $z \sim 5$  is less than  $0.1 \text{ h}^{-1} \text{ Mpc}$  and increases to  $\sim 1 \text{ h}^{-1} \text{ Mpc}$  at  $z \sim 2$ .

Quasar's Ly $\alpha$  absorption spectra at high redshift  $z \sim 5 - 6$  are significantly different from that at low redshift  $z \sim 2 - 3$ . The latter show Ly $\alpha$  forests, while the former consist of complete absorption troughs (Gunn-Peterson troughs) separated by tiny transparent regions. In other words, Ly $\alpha$  transmitted flux experience a strong evolution with redshift rising from  $z \sim 2 - 3$  to  $5 - 6$ . The low-order statistics of the Ly $\alpha$  transmitted flux, such as the mean optical depth and its variance, also show strong redshift evolution. Therefore, the weak redshift-evolution of  $\beta$  is very interesting. It implies that the  $\beta$  non-Gaussian feature is mainly dependent on the nonlinear state of the fluid, but weakly dependent on the optical depth and its variance.

### 3.3 Non-Gaussianity related to parameter $\gamma$

We now turn to the  $\gamma$ -related non-Gaussianity, which is given by (Liu & Fang 2008)

$$\ln \frac{\langle \delta\tau_r^{2p} \rangle}{\langle \delta\tau_r^2 \rangle^p} = K_p \ln r + \text{const}, \quad (14)$$

and

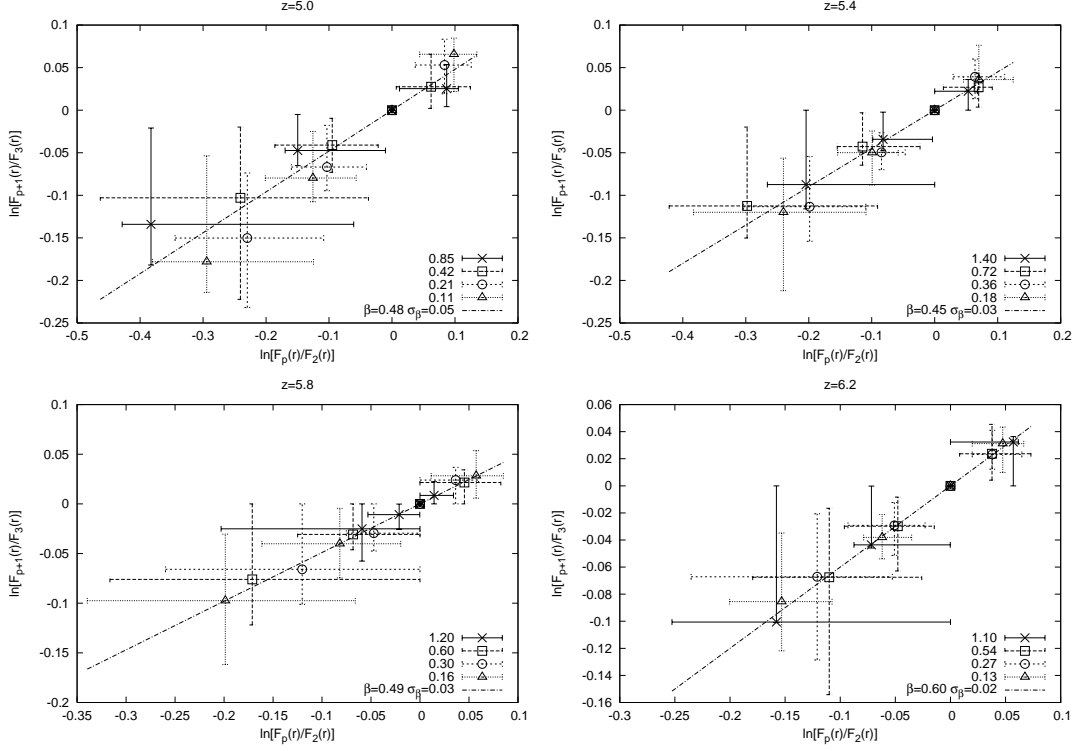


**Figure 2.** The  $\beta$ -hierarchy of observed sample of the Ly $\alpha$  transmitted flux at redshift  $z = 5.0$  (top-left),  $5.4$  (top-right),  $5.8$  (bottom-left) and  $6.2$  (bottom-right). The physical scale  $r$  is in the range  $\sim 0.1 - 1.5 h^{-1}$  Mpc, and order  $p$  is from 1 to 2.5. The error bars are given by the maximum and minimum of bootstrap re-sampling.

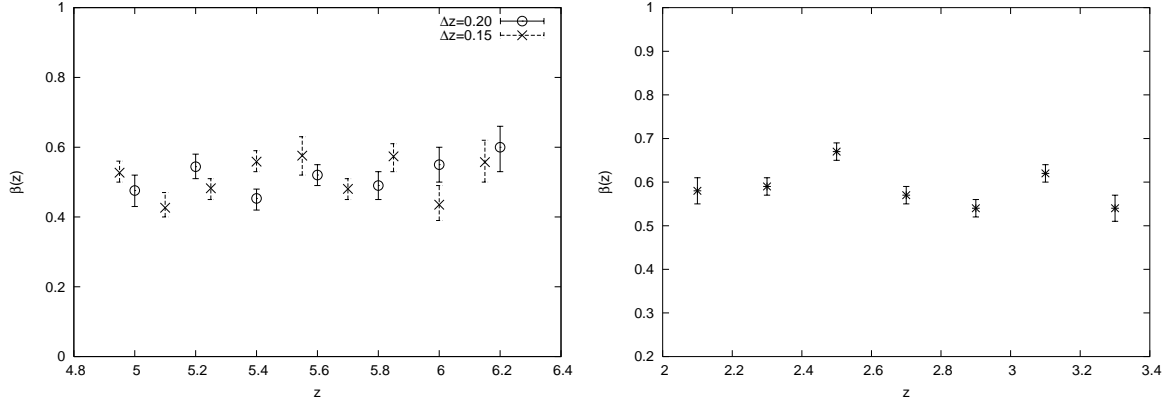


**Figure 3.** Redshift dependence of parameter  $\beta$  for samples of a.) Fan et al (2006) (left), and b.) the Keck HIREs quasars, Jamkhedkar et al.(2003) (right).

$$K_p = -\gamma \frac{p(1 - \beta^2) - (1 - \beta^{2p})}{1 - \beta}. \quad (15)$$

It requires that for a given  $p$ , the relation  $\ln \langle (\delta\tau_r)^{2p} \rangle / \langle (\delta\tau_r)^2 \rangle^p$  and  $\ln r$  has to be a straight line with slope  $K_p$ . Since parameter  $\beta$  is already determined by  $\beta$ -hierarchy in last section, we can then figure out the parameter  $\gamma$  from  $K_p$ .

The result is presented in Figure 4. It shows the relation of  $\ln \langle (\delta\tau_r)^{2p} \rangle / \langle (\delta\tau_r)^2 \rangle^p$  vs.  $\ln r$  for observational data at redshift ranges  $z = 5.0, 5.4, 5.8$  and  $6.2$ . The order parameter  $p$  is set to 2 and 3, i.e. the statistics of eqs.(14) and (15) are of the order of 4 and 6. The error bars are given by the maximum and minimum of each  $r$ . The  $\ln r$ -dependency of  $\ln \langle (\delta\tau_r)^{2p} \rangle / \langle (\delta\tau_r)^2 \rangle^p$  approximately at each range can be given by a straight line.

The slopes  $K_p$  of the straight lines of Figure 4 are listed in Table 1, and parameter  $\gamma$  given by eq.(15) is also listed. In log-Poisson hierarchy, parameter  $\gamma$  has to be independent of  $p$  and therefore, the values of  $\gamma$  determined by  $K_p$  with different straight lines should be the same. Table 1 indeed confirms this point. We see that for a given redshift, the statistics of  $p = 2$  and 3 yield the same  $\gamma$  within their errors. Therefore, the high redshift Ly $\alpha$  transmitted flux well fulfills the  $\gamma$ -related non-Gaussianity.

A basic feature of log-Poisson model is to yield nonlinear terms of  $p$ , i.e. the term  $\beta^p$  in eq.(7) and  $\beta^{2p}$  in eq.(15) (Frisch 1995). The terms with linear  $p$  can also be given by other models. Since  $\beta < 1$ , the tests with  $\beta^n$  and  $n > 6$  don't give new test on the log-Poisson model. Therefore, the statistical order  $n$  generally is taken to be less than 6.

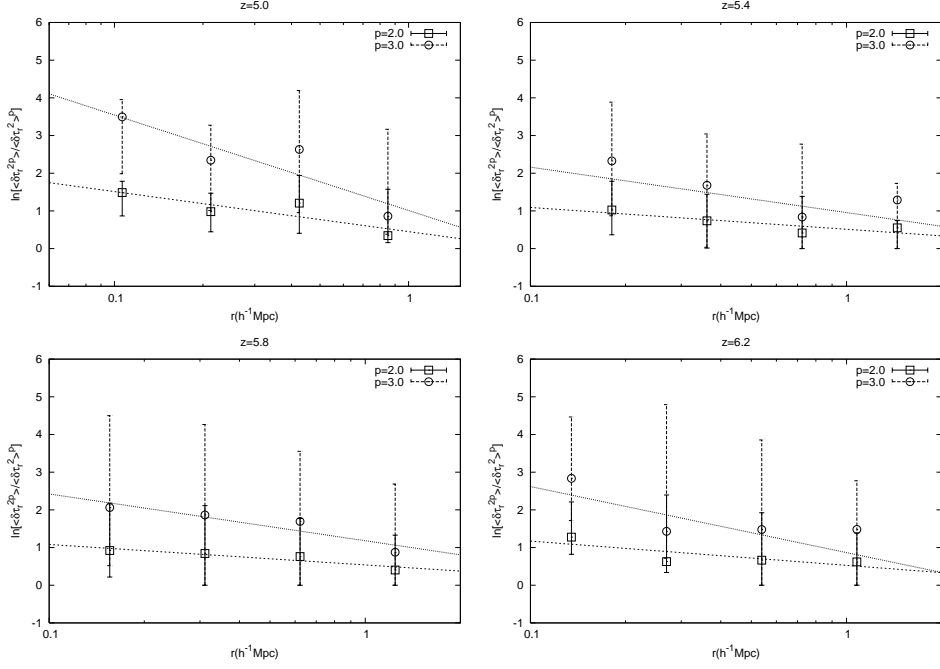


**Figure 4.**  $\ln[\langle(\delta\tau_r)^{2p}\rangle/\langle(\delta\tau_r)^2\rangle^p]$  vs.  $r$  of observed sample of the Ly $\alpha$  transmitted flux for redshifts at 5.0 (top-left), 5.4 (top-right), 5.8 (bottom-left), and 6.2 (bottom-right).  $p$  is taken to be 2 (bottom line) and 3 (top line). The solid lines are given by the least square fitting. The error bars are given by the maximum and minimum of bootstrap re-sampling.

Table 1. Parameter  $\gamma$  at redshift  $z = 5.0$  to 6.2

$z$	$p$	$K_p$	$\gamma$
5.0	2	$-0.46 \pm 0.20$	$0.41^{+0.17}_{-0.18}$
	3	$-1.10 \pm 0.40$	$0.43^{+0.16}_{-0.15}$
5.4	2	$-0.25 \pm 0.10$	$0.22^{+0.08}_{-0.07}$
	3	$-0.52 \pm 0.30$	$0.20^{+0.12}_{-0.11}$
5.8	2	$-0.24 \pm 0.07$	$0.21^{+0.06}_{-0.06}$
	3	$-0.52 \pm 0.15$	$0.21^{+0.06}_{-0.06}$
6.2	2	$-0.28 \pm 0.16$	$0.27^{+0.15}_{-0.15}$
	3	$-0.78 \pm 0.35$	$0.31^{+0.13}_{-0.12}$

#### 4 HYDRODYNAMIC SIMULATION SAMPLES

Although the mean optical depth and its variance of Ly $\alpha$  transmitted flux of quasar's absorption spectrum underwent a strong evolution at high redshift, the log-Poisson non-Gaussianity, as last section reveals, shows only weak dependence on redshift. Thus, an important question is whether the two aspects of the redshift evolutions can be conciliated within the concordance  $\Lambda$ CDM model. We study this problem with cosmological hydrodynamic simulation samples.

##### 4.1 Simulation samples of neutral hydrogen

We first produce the samples of mass density, temperature and velocity fields of cosmic hydrogen with hydrodynamic simulation with the same code of Liu et al. (2007, 2008), which is based on Eulerian method for hydrodynamics with 5th order Weighted Essentially Non-oscillatory (WENO) finite difference scheme and particle mesh(PM) method for dark matter particles (Feng et al. 2004). We use cosmological parameters given by the latest result of WMAP (Komatsu et al. 2009). We run simulations in a period box

of side  $25h^{-1}$  Mpc with  $512^3$  grids and dark matter particles which have a mass resolution of  $1.04 \times 10^7 M_\odot$ . Assuming ionization equilibrium, atomic processes, including radiative cooling, heating and fraction of species, are modeled using the primordial composition ( $X = 0.76, Y = 0.24$ ) and formalism in the Appendix of Theuns et al. (1998), under optically thin approximation. Photoionization and photoheating are switched on after the UV background is added at  $z = 11.0$ .

Started at  $z = 99$ , a sample output at  $z = 11$  first. Simulations with different UV histories are then performed from this snapshot at  $z = 11$  and produce snapshots at redshifts from  $z = 6.5$  to  $z = 4.9$  at a interval of  $\Delta z = 0.1$ . As we focus on the evolution at high redshifts, simulations are stopped at  $z = 4$ . From snapshot dumps, we produce the mass density field of hydrogen  $\rho(\mathbf{x})$ , temperature field  $T(\mathbf{x})$ , and velocity field  $\mathbf{v}(\mathbf{x})$ . Star formation is not included. However, the contribution of stars to the UV background is considered by fitting the redshift evolution of the UV background with mean optical depth and its variance of Ly $\alpha$  transmitted flux field. This code has recently been used to produce samples to show the turbulence behavior at redshift as high as  $z \simeq 4$  (Zhu et al. 2010). These samples would also be suitable to test the log-Poisson non-Gaussianity of the IGM at high redshifts.

Although the Gunn-Peterson optical depth shows dramatic decrease with redshift and abnormally large scatter at  $z \sim 6$ , it can still be fitted by models of a uniform ionizing background (Lidz et al. 2006; Liu et al. 2006, 2007; Mesinger & Furlanetto 2009). As current observation does not give a well knowledge of ionizing source at high redshift, instead of the Haardt & Madau (2001) model of UV background history, we use a more general uniform UV background with the ionizing photons have a power-law spectrum with index  $-1.0$  and an normalized coefficient  $J_{21}$ . The hydrogen photoionization rate  $\Gamma_{-12}$  is calculated using the fitting formula in Theuns et al. (1998) and then is used to calculating the

heating and cooling in the hydrodynamic simulation. The photoionization rate can be given by

$$\Gamma_{-12} = 3.15 J_{21}. \quad (16)$$

Based on the above assumption, the history of the UV background in our simulation is given by the evolution of  $J_{21}$ . There is no direct observation on this parameter. Considering the two typical reionization history in references, one is the extended scenario and the other is phase transition, we use the following two redshift-dependent models of  $J_{21}$ ,

$$J_{21}(z) = 5.0 \times \exp(-0.475z). \quad (17)$$

$$J_{21}(z) = \exp(-0.21z^2 + 1.5z - 3.0) + 0.02 \exp(-7.0/z). \quad (18)$$

The  $J_{21}(z)$  of eq.(17) can be considered as a model of the extended reionization scenario. Eq.(18) gives approximately the same evolution as eq.(17) at  $z = 4.0 - 5.0$ , but drops about an order of magnitude from  $z = 5.0$  to  $z = 7.0$  and stays at very low level when  $z > 7$ . It is to mimic the reionization as a phase transition over redshift range from  $z = 5.0$  to  $z = 7.0$ . The parameters used in eqs.(17) and (18) actually are determined by the fitting of simulated samples with observed mean optical depth and its variance of Ly $\alpha$  transmitted flux field. Several simulations have been performed before these parameters are selected. It is interesting to see that with the parameters of eqs.(17) and (18), the intensities of  $\Gamma_{-12}$  given by eq.(16) in the redshift range  $z = 4 - 9$  are just in between of the values given by 1.) Haardt & Madau, (2001) and 2.) proximity effect of quasars (Dall'Aglio et al. 2008, Gilmore et al. 2009 and references therein ).

The last but not least, although the intensities of the UV background given by models (17) and (18) are very different at  $z = 5.0$  to  $z = 7.0$ , the non-Gaussian features of the transmitted field of Ly $\alpha$  are less affected. This is because the basic variable  $\delta\tau_r = \tau(x+r) - \tau(x)$  is not sensitive to the change of the uniform ionizing background given by the models (17) and (18), especially when  $r$  is small.

## 4.2 Intermittence of neutral hydrogen density field

Before simulating the Ly $\alpha$  transmitted flux, we analyze the log-Poisson behavior of the simulation samples of neutral hydrogen density field,  $n_{\text{HI}}(\mathbf{x})$ . We first calculate the  $\beta$ -hierarchy of neutral hydrogen field. The results are presented in Figure 5, which contains all data points of  $F_{p+1}(r)/F_3(r)$  and  $F_p(r)/F_2(r)$  with  $p = 1, 1.5, 2$ , and  $2.5$ , and available scale  $r$ . To estimate errors, we divide our 160 one-dimensional samples into 80 subsamples, each of which has 2 lines. The error bars are given by the scattering ranges of the 80 subsamples. Figure 5 shows that  $\beta$ -hierarchy is also well hold for neutral hydrogen density field. The numbers of  $\beta$  are also shown in Figure 5. It is in the range  $3.0 - 3.5$ .

In log-Poisson hierarchy, the  $r$ -dependence of  $F_p(r)$  is given by (Liu et al 2008; Lu et al. 2009)

$$F_p(r) = Ar^{-\alpha-\gamma(1-\beta^p)}. \quad (19)$$

That is, the relation between  $\ln F_p(r)$  and  $\ln r$  should be a straight line with the slope  $-\alpha+\gamma(1-\beta^p)$ . For Gaussian field we have  $\beta = 1$ , and therefore, the slope is independent of  $p$ . For log-Poisson field ( $\beta < 1$ ), when  $p$  is large, the slope converges to  $-(\alpha-\gamma)$ . On the other hand, parameter  $\alpha$  can be determined by the power spectrum of  $n_{\text{HI}}(x)$  (§2.2). Thus, The  $\ln F_p(r)$ - $r$  relation with larger  $p$  can be used to determine parameter  $\gamma$ .

Figure 6 presents  $\ln F_p(r)$  vs.  $\ln r$  of the simulation samples

of neutral hydrogen mass density field in the physical length scale range of  $0.1 < r < 1.5 \text{ h}^{-1} \text{ Mpc}$  and orders of  $p = 0.5 \times n$  with  $n = 1, 2, \dots, 8$ . For all redshifts and  $p \leq 4$ ,  $\ln F_p(r) - \ln r$  can indeed be approximately fitted by straight lines. These straight lines have different slopes. The higher the  $p$ , the more steeper the straight lines are. It implies that  $\beta < 1$  and the density fields are non-Gaussian. When  $p > 3$ , the fitted straight lines are almost independent of  $p$ . It shows the convergent of the slope to  $-(\alpha-\gamma)$  at high  $p$ . The parameters  $\gamma$  found with slope of  $\ln F_p(r)$ - $r$  lines are 0.70, 0.65, 0.60 and 0.60, corresponding to redshifts  $z = 5.0, 5.4, 5.8$  and  $6.2$  respectively.

From the parameters  $\beta$  and  $\gamma$  given above, we plot the intermittent exponent  $\xi(p)$  [eq.(8)] in Figure 7, in which data points are given by fitting structure functions of simulation samples to eq.(2) with  $p = 0.5 + 0.5n$ ,  $n = 0 \dots 11$ . As mentioned in §3.3, the test is limited in the range  $p \leq 6$ . The error bars of Figure 7 are given by the maximum and minimum of the 80 subsamples.

One can conclude that the fields of neutral hydrogen mass density can be well described by the She-Leveque's scaling formula with statistical order as high as  $p = 6$ . It should be noted again, Figure 7 covers the physical scales from  $\sim 0.1$  to  $1.5 \text{ h}^{-1} \text{ Mpc}$ . It indicates that cosmic neutral hydrogen fluid is turbulent on the scales considered.

## 5 CONFRONTATION OF OBSERVED DATA WITH SIMULATION SAMPLES

### 5.1 Ly $\alpha$ spectrum synthesise

Assuming ionization equilibrium under the uniform UV background, we generate the field of neutral hydrogen fraction  $f_{\text{HI}}(\mathbf{x}) = n_{\text{HI}}(\mathbf{x})/n_{\text{H}}(\mathbf{x})$  at each cell, where  $n_{\text{H}}(\mathbf{x})$  and  $n_{\text{HI}}(\mathbf{x})$  are, respectively, the number densities of hydrogen and neutral hydrogen at  $\mathbf{x}$ . We synthesize 160 samples of normalized Ly $\alpha$  transmitted flux  $\mathbb{F}(z) = \exp[-\tau(z)]$  from  $z = 4.9$  to  $z = 6.3$  using the same methods as Zhang et al (1997) and Paschos & Norman (2005). The optical depth  $\tau(z)$  is given by

$$\tau(z) = \frac{\sigma_0 c}{H} \int_{-\infty}^{\infty} n_{\text{HI}}(x) V[z - x - v(x), b(x)] dx, \quad (20)$$

in which  $\sigma_0$  is the effective cross-section of the resonant absorption and  $H$  is the Hubble constant at corresponding redshifts of the samples. The Voigt function is  $V[z - x - v(x), b(x)] = 1/(\pi^{1/2}b) \exp\{-[z - x - v(x)]^2/b^2(x)\}$ , where  $b(x)$  gives the thermal broadening.

Along an randomly selected lines of sight, we synthesize an absorption spectrum  $\mathbb{F}$  from  $z = 4.9$  to  $6.3$  by dividing the spectrum into redshift intervals of  $\Delta z = 0.1$ . As the corresponding physical length scale for this redshift interval is larger than our simulation box size, we integrate eq. (20) over the simulation dump periodically. Each spectrum is resolved with the same resolution of observation. Gaussian noise is added with signal-to-noise ratio  $S/N = 10$ .

We calculate the Gunn-Peterson optical depth and its dispersion of the 160 synthesized samples. The results are shown in Figure 8. The observed results (Fan et al. 2006) are also shown in the Figure. The simulation samples basically are consistent with the observations except the dispersion at redshift  $z = 6.2$ . The deviation at redshift  $z = 6.2$  might be due to the available observed samples at the redshift range  $z \sim 6.2$  is too few.

We also do the statistics of the probability distribution function of the transmitted flux  $\mathbb{F}(z)$  of observation and simulation from

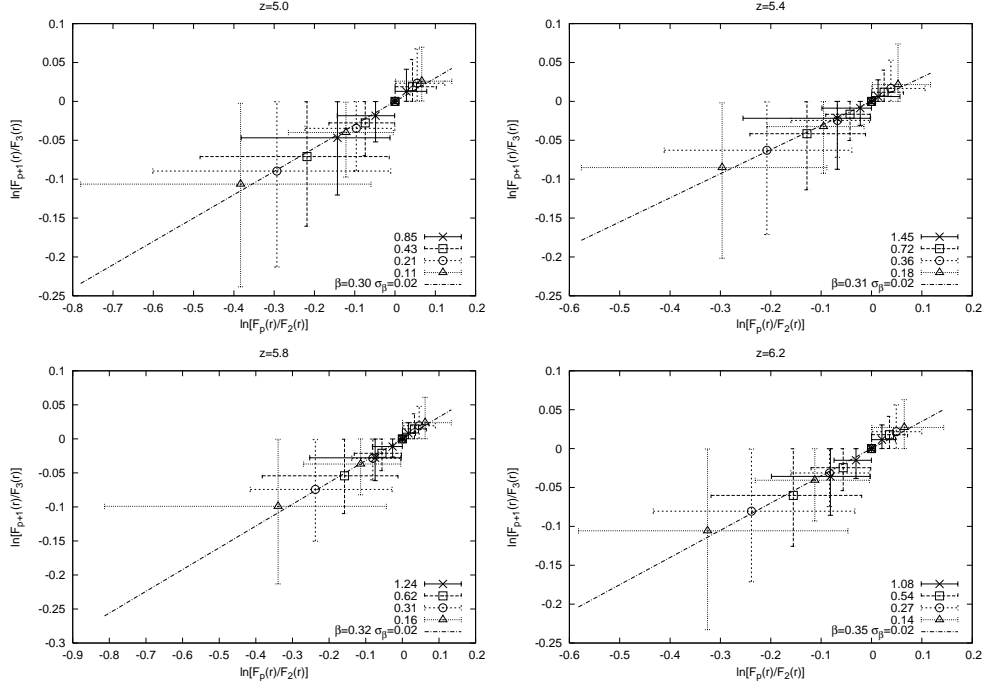


**Figure 5.**  $\ln[F_{p+1}(r)/F_3(r)]$  vs.  $\ln[F_p(r)/F_2(r)]$  for simulation samples of the mass density field of neutral hydrogen at redshifts 5.0, 5.4, 5.8, 6.2. The statistical order to be  $p = 1, 1.5, 2$ , and  $2.5$ .

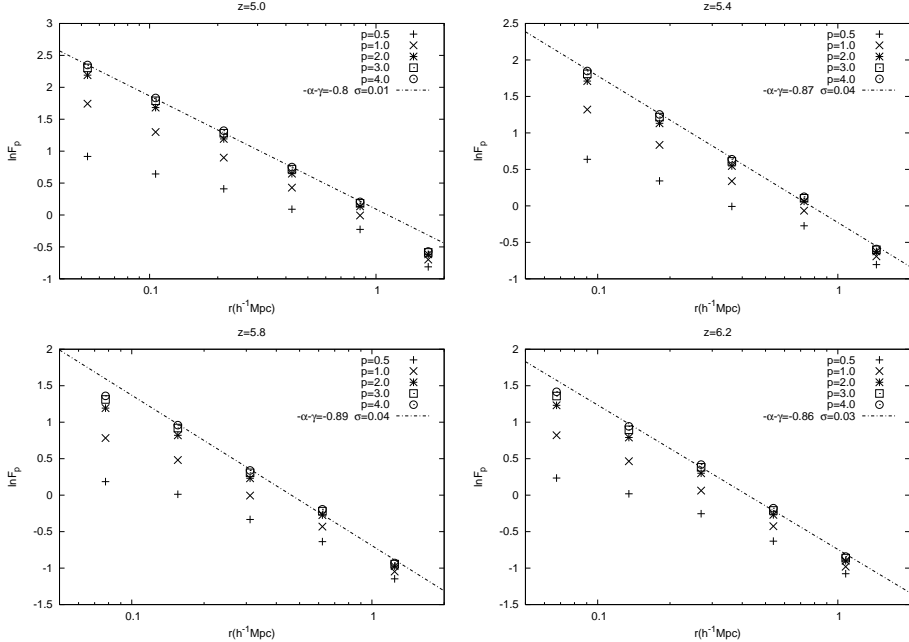


**Figure 6.**  $\ln F_p(r)$  vs.  $\ln r$  of simulation samples of neutral hydrogen mass density field. The number  $\gamma$  is given in each panel.

$z = 5.3$  to  $z = 6.1$ . The results are presented in Figure 9. The PDF of simulation samples can also fit observations within 1-sigma range. Thus, all low order statistics of the simulated samples are consistent with observation.

## 5.2 Redshift dependence of $\beta$

Using the method of §3.2, we calculate the parameters  $\beta$  of simulated samples of Ly $\alpha$  spectra. To mimic the observation samples,

which contains totally 19 lines, we divide 160 one-dimensional simulation samples into 8 subsamples, each of which has 20 1-D samples. The uniform UV background eq.(17) and eq.(18) are used to produce the simulation samples. Figure 10 presents the redshift dependence of parameter  $\beta$  for observed data and simulation samples. The error bars of the simulation results are given by the maximum and minimum of the 8 subsamples.

Although the redshift-dependence of the UV background eqs.(17) and (18) are different at  $z > 5$ , Figure 10 shows that



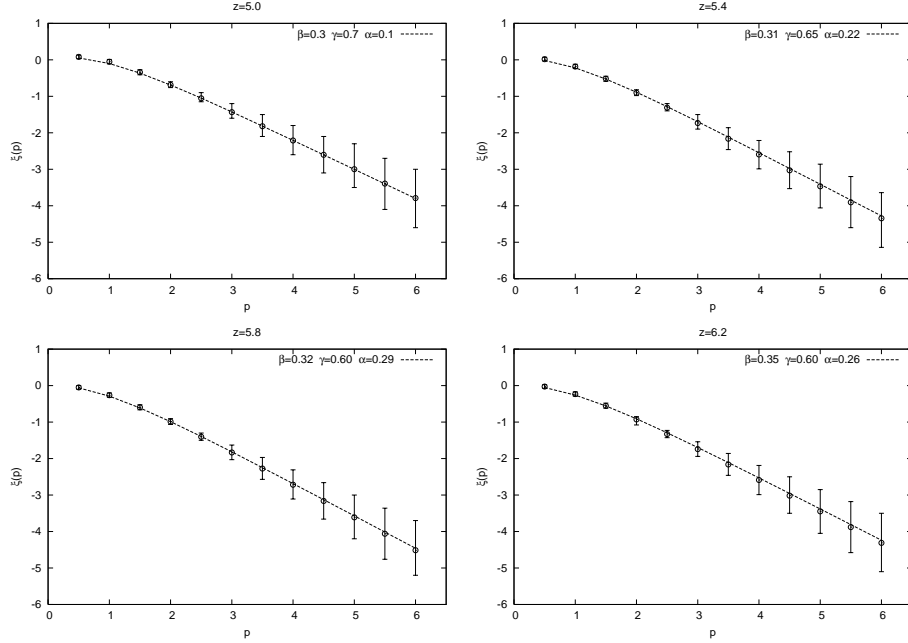


**Figure 7.** Intermittent exponent  $\xi(p)$  of simulation samples of the mass density field of neutral hydrogen. The error bars are the variance of  $\xi(p)$  over 80 sub-samples, each of which contains of 2 one-dimensional samples.

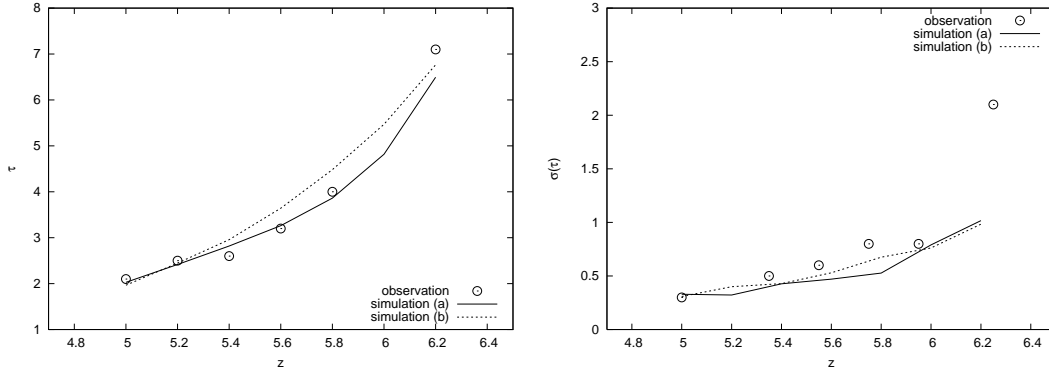


**Figure 8.** Redshift-dependence of mean optical depth (left) and its variance (right). It shows observed result (circle) and simulation samples with UV background eq.(17) (solid line) and eq.(18) (dotted line).

the redshift-dependence of  $\beta$  given by the two models are about the same. It is because the uniform field  $J_{21}$  would not change the non-Gaussianity significantly. The simulation results of parameter  $\beta$  are basically consistent with the observation, only at  $z = 5.4$  shows a small deviation. Therefore, the  $\Lambda$ CDM universe embedded with a uniform UV background history is able to explain the feature of  $\beta$  redshift-revolution.

Figure 7 shows that the parameters  $\beta$  of neutral hydrogen density field is in the range  $0.30 - 0.35$ , which is much less than the results shown in Figure 10. It indicates that the non-Gaussianity of neutral hydrogen field is different from that of Ly $\alpha$  transmitted flux. This is because the non-Gaussianity of Ly $\alpha$  transmitted flux depends not only on the mass density field of neutral hydrogen, but also on the velocity field via the Voigt convolution eq.(20).

### 5.3 Parameter $\gamma$

Similar to §3.3, we use high order moment  $\langle \delta\tau_r^{2p} \rangle$  to quantify  $K_p$  (eq.(15)) and then the parameter  $\gamma$ . The results are listed in Table 2. The values of  $\gamma$  for  $p = 2$  and  $3$  in each  $z$  range are the same within their errors. Comparing Table 1 and 2, the parameter  $\gamma$  given by observation data and simulation sample are also consistent with each other within their errors.

The parameter  $\gamma$  for observational samples of Ly $\alpha$  transmitted flux at  $z = 2.5$  is found to be  $0.58 \pm 0.20$  (Lu et al 2009), which is higher than that listed in Table 2. It might indicate that parameter  $\gamma$  is decreasing with redshift. However, we should keep in mind that the error bars of observational sample are large both at high and low redshift, the redshift evolution of parameter  $\gamma$  is not certain yet.

Figure 6 reveals that parameter  $\gamma$  of neutral hydrogen is in the range  $0.80 - 0.89$ , which is much larger than that shown in Tables 1 and 2. Parameter  $\gamma$  measures the singular structures and higher  $\gamma$  represents stronger singularity (Liu & Fang, 2008; Lu et al 2009). Therefore, the field of neutral hydrogen mass density con-

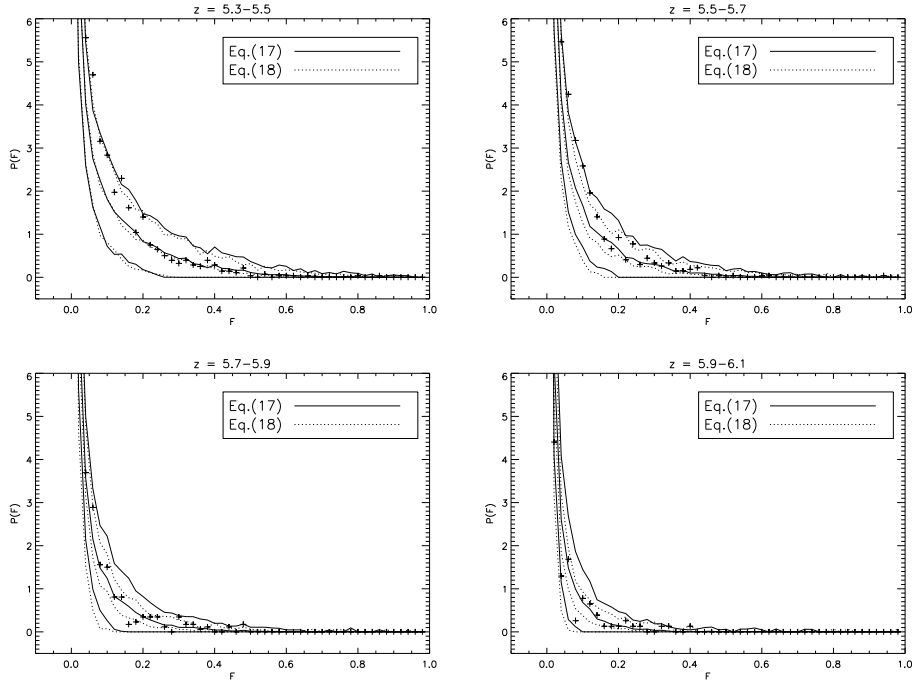


**Figure 9.** Probability distribution functions of the transmitted flux at  $z = 5.3 - 5.5$  (top left),  $z = 5.5 - 5.7$  (top right),  $z = 5.7 - 5.9$  (bottom left),  $z = 5.9 - 6.1$  (bottom right). Cross are observation data. The solid and dashed line in the center are results of samples generated with eq.(17) and eq.(18) respectively. The above and below set of lines gives the  $1\sigma$  errors.

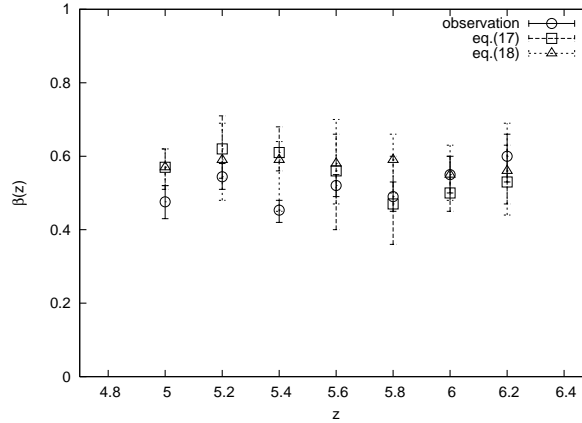


**Figure 10.** Parameter  $\beta$  vs. redshift for real data of Ly $\alpha$  transmitted flux (§3.2)(circle); and hydrodynamic simulation results samples with UV background eq.(17) (square), and eq.(18) (trigon).

tains much more singular structures than that of Ly $\alpha$  transmitted flux.

#### 5.4 Spatially non-uniform UV background

Whether the UV background at redshift  $z \sim 5 - 6$  is spatially uniform is an important problem of the history of reionization. With only the redshift evolution of the optical depth and its variance at  $z \sim 5 - 6$ , it seems to be difficult to distinguish models with uniform background from inhomogeneous one. We will explore whether the log-Poisson non-Gaussian feature is dependent on the inhomogeneity of the UV background.

Many works have been done on the fluctuation of hydrogen-

ionizing radiation background field. Analytical method and Monte Carlo simulations with randomly distributed sources were firstly used to estimate the intensity fluctuations and its effect on the Ly $\alpha$  forest (Zuo 1992; Fardal & Shull 1993; Croft et al. 1999). Large scale N-body simulations and hydrodynamical simulations then were applied to study the fluctuations of the UV background (Gnedin & Hamilton 2002; Meiksin & White 2003; Meiksin & White 2004; Croft 2004; Bolton et al. 2006). Investigations have been carried out recently on this problem at high redshift (Wyithe & Loeb 2005; Mesinger & Furlanetto, 2009; Furlanetto & Mesinger 2009). The general features of an inhomogeneous UV background can be sketched as

$$J_{21}(\mathbf{x}, z) = \bar{J}_{21}(z)[1 + \delta(\mathbf{x}, z)], \quad (21)$$

Table 3. Parameter  $\beta$  and UV background models

$z$	A	B	C	D
5.4	$0.48 \pm 0.02$	$0.57 \pm 0.02$	$0.56 \pm 0.02$	$0.55 \pm 0.02$
5.8	$0.52 \pm 0.02$	$0.50 \pm 0.02$	$0.53 \pm 0.02$	$0.52 \pm 0.02$

Table 2. Parameter  $\gamma$  at redshift  $z = 5.0$  to  $6.2$ 

$z$	$p$	$K_p$	$\gamma$
5.0	2	$-0.29 \pm 0.04$	$0.27^{+0.04}_{-0.04}$
	3	$-1.71 \pm 0.06$	$0.29^{+0.02}_{-0.03}$
5.4	2	$-0.29 \pm 0.06$	$0.29^{+0.06}_{-0.05}$
	3	$-0.73 \pm 0.12$	$0.30^{+0.05}_{-0.04}$
5.8	2	$-0.23 \pm 0.03$	$0.20^{+0.03}_{-0.03}$
	3	$-0.59 \pm 0.07$	$0.23^{+0.03}_{-0.03}$
6.2	2	$-0.15 \pm 0.11$	$0.14^{+0.10}_{-0.10}$
	3	$-0.38 \pm 0.24$	$0.15^{+0.09}_{-0.10}$

where  $\bar{J}_{21}(z)$  is the UV background given by eqs.(17) or (18). Equation (21) means, the field of the UV background is fluctuated with respect to its mean  $\bar{J}_{21}(z)$ .

Unfortunately, no commonly accepted  $J_{21}(\mathbf{x}, z)$  or  $\delta(\mathbf{x}, z)$  are available. The fluctuation field  $\delta(\mathbf{x}, z)$  may or may not be correlated with the density distribution of cosmic baryon matter. In this context, we consider 4 toy models of  $\delta(\mathbf{x})$  as follows:

- A.  $\delta(\mathbf{x}) = 0.1g(\mathbf{x})$ , where  $g(\mathbf{x})$  is a Gaussian random field with variance  $\sigma^2 = 1.0$ .
- B.  $\delta(\mathbf{x}) = 0.3g(\mathbf{x})$ .
- C.  $\delta(\mathbf{x})$  is given by

$$\delta(\mathbf{x}) = \begin{cases} \delta_0 \sin(\frac{\pi}{2} \min(\lg(\rho(\mathbf{x}))/2.0, 1.0)) & \rho(\mathbf{x}) > 1.0 \\ \delta_0(\frac{\pi}{2} \max(\lg(\rho(\mathbf{x}))/2.0, -1.0)) & \rho(\mathbf{x}) < 1.0 \end{cases} \quad (22)$$

where  $\delta_0 = 0.1$ .

- D. The same as model C, but  $\delta_0 = 0.3$ .

For models A and B, the fluctuations of UV background are statistically independent of the IGM density field, while it is correlated to the IGM distribution for models C and D.

Because the radiative transfer has not yet been included in our simulation, we simply add the non-uniform UV background to the outputs of simulations with eq.(17) and produce samples of the neutral hydrogen density field and Ly $\alpha$  transmitted flux at redshift 5.4 and 5.8. Since our goal is only to see whether the non-Gaussianity is affected by a fluctuating UV background, the post processing method would be acceptable as a first try.

The  $\beta$  values of the Ly $\alpha$  transmitted flux samples based on non-uniform UV background eq.(22) are listed in Table 3. Although the  $\beta$  values among models A,B,C and D sometimes show 1- $\sigma$  deviation from each other, these simplified models seem to have no effect in general. It may indicate that the effect of inhomogeneous UV background on the log-Poisson non-Gaussian feature is not detectable yet with current data.

## 6 DISCUSSION AND CONCLUSION

Nonlinear evolution of baryon fluid at high redshift is a central problem of cosmology. It is well known that in the nonlinear regime the dynamical behavior of cosmic baryon fluid does not always

trace the collisionless dark matter. The non-Gaussianity of the mass and velocity fields of baryon fluid is given by the hydrodynamics of the cosmic flow. A common property of the evolution of a Navier-Stokes fluid is to reach a turbulent state when the Reynolds number is high (e.g. Zhu et al. 2010). In the scale free range, the fully developed turbulence is of statistically quasi-steady characterized by log-Poisson hierarchy. In this regime, the cosmic baryon fluid undergoes the evolution of clustering and finally falls into massive halos of dark matter to form structures, including light-emitting objects.

The cosmic baryon fluid or the IGM, both at high and low redshifts, exhibits the log-Poisson non-Gaussian features in the range from the onset scale of the nonlinear evolution to the dissipation scale, i.e. the Jeans length. The log-Poisson non-Gaussianity has been identified in various simulated and observed samples of the IGM, including the mass density and velocity fields of baryonic matter, the density field of neutral hydrogen, and Ly $\alpha$  transmitted flux. Although these fields are different from each other, they show the common behavior of log-Poisson non-Gaussianity. This scenario is further supported with high redshift Ly $\alpha$  transmitted flux.

The log-Poisson non-Gaussian parameter  $\beta$  of the mass density field on the same physical scales is found to be increasing with redshift (Liu & Fang 2008). It implies that the mass density field of the IGM is less non-Gaussian at high redshifts. The log-Poisson non-Gaussianity at high redshifts should be weak than that of low redshifts on the same physical scale. However, we found in this paper that observed data of Ly $\alpha$  transmitted flux at redshift  $z = 5 - 6$  shows about the same level of log-Poisson non-Gaussianity as low redshift  $z \sim 2$  data. This is because the scales covered by the data at  $z = 5 - 6$  are smaller than the data at  $z \sim 2$ . The weak evolution of  $\beta$  given by this paper implies that turbulence state of cosmic baryon fluid at  $z \sim 2$  on physical scales  $1 - 10 \text{ h}^{-1} \text{ Mpc}$  is about the same as that at  $z = 5 - 6$  on physical scales  $0.1 - 1 \text{ h}^{-1} \text{ Mpc}$ . This is reasonable considering that the Jeans length and the typical scale of onset of nonlinear evolution are increasing with time. The log-Poisson non-Gaussianity at low and high redshifts are about the same once the nonlinear evolution is fully developed.

In a word, on the scales of fully developed turbulence, the parameter  $\beta$  of the IGM at high and low redshifts should be about the same. This property is very different from the Gunn-Peterson optical depth and its variance, both show a strong redshift dependence. The Gunn-Peterson optical depth and its variance are sensitive to the intensity of the UV background. Oppositely, the parameters of the log-Poisson non-Gaussianity are weakly dependent on the intensity of the UV background. A more self-consistent and delicate handle of the inhomogeneity of the UV background in the cosmic hydrodynamic simulation and much more high quality observation data would help us to use the log-Poisson non-Gaussianity to investigate the ionizing background at high redshift.

## 7 ACKNOWLEDGMENTS

WSZ acknowledges the support of the International Center for Relativistic Center Network (ICRANet).

## REFERENCES

- Becker, G.D., Rauch, M. & Sargent, Wallace L.W., 2007, *ApJ*, 662, 72B
- Benzi, R., Biferale, L. & Trovatore, E., 1996, *Phys. Rev. Lett.* 77, 3114
- Bi, H. G., 1993, *ApJ*, 405, 479
- Bi, H.G. & Davidsen, A.F. 1997, *ApJ*, 479, 523
- Bolton J. S., Haehnelt M. G., Viel M., Carswell R. F., 2006, *MNRAS*, 366, 1378
- Cole, S. & Kaiser, N. 1988, *MNRAS*, 233, 637
- Croft, R. A. C., Weinberg, D. H., Pettini, M., Hernquist, L., & Katz, N. 1999, *ApJ*, 520, 1
- Croft R. A. C., 2004, *ApJ*, 610, 642
- Dall'Aglio A., Wisotzki L., Worseck G., 2008, *A&A*, 491, 465
- Donoho D. L., 1995, *IEEE Trans. Inf. Theory*, 41, 613
- Dubrulle, B. 1994, *Phys. Rev. Lett.* 73, 959
- Fan, X. et al. 2002, *AJ*, 123, 1247
- Fan, X. et al. 2006, *AJ*, 132, 117
- Fardal M. A., Shull J. M., 1993, *ApJ*, 415, 524
- Feng, L.L. & Fang, L.Z. 2000, *ApJ*, 535, 519
- Feng, L.L., Pando, J. & Fang, L.Z. 2001, *ApJ*, 555, 74
- Feng, L.L., Shu, C.W., & Zhang, M.P. 2004, *ApJ*, 612, 1
- Feng, L.L., Bi, H.G., Liu, J., Fang, L.Z., 2008, *MNRAS*, 383, 1459F
- Frisch, U. 1995, *Turbulence* (Cambridge press)
- Furlanetto, S., Mesinger, A., 2009, *MNRAS*, 394, 1667
- Gallerani, S., Ferrara, A., Fan, X., Choudhury, T.R. & Salvaterra, R., 2007, *NCimB*, 122, 977G
- Gnedin N. Y., Hamilton A. J. S., 2002, *MNRAS*, 334, 107
- Gilmore, R. C., Madua, P., Primack, J. R., Somerville, R. S., & Haardt, F., 2009, *MNRAS* 399, 1694
- Haardt, F., Madau, P. 2001, in *Proc. XXXV Rencontres Moriond, Galaxy Clusters and the High Redshift Universe*, ed. D. M. Neumann & J. T. T. Van (Gif-sur-Yvette: Editions Frontie' res)
- He, P., Liu, J.R., Feng, L.L., Shu, C.W. & Fang, L.Z. 2006, *Phys. Rev. Lett.* 96, 051302
- Jamkhedkar, P., Bi, H.G. & Fang, L.Z., 2001, *ApJ* 561, 94
- Jamkhedkar, P., 2002, *Intermittency in Large Scale Structures in the Universe*, Ph.D. thesis, University of Arizona, Tucson
- Jamkhedkar, P., Feng, L.L., Zheng, W., Kirkman, D., Tytler, D., & Fang, L.Z., 2003, *MNRAS*, 343, 1110
- Kirkman, D. & Tytler, D., 1997, *ApJ* 484, 672
- Komatsu, E., et al. 2009, *ApJS*, 180, 330
- Leveque, E. & She, Z.-S. 1997, *Phys. Rev. E* 55, 2789
- Lidz, A., Oh, S. P. & Furlanetto, R. 2006, *ApJ*, 639, L47
- Liu, J., Bi, H.G., Feng, L.L., & Fang, L.Z. 2006, *ApJ*, 645, L1
- Liu, J., Bi, H.G. & Fang, L.Z. 2007, *ApJ*, 671, L89
- Liu, J. & Fang, L. Z. 2008, *ApJ*, 672, 11
- Liu, J., Jamkhedkar, P., Zheng, W., Feng, L. L., & Fang, L. Z. 2006, *ApJ*, 645, 861
- Lu, Y., Chu, Y. Q. & Fang, L. Z. 2009, *ApJ*, 691, 43-53
- Meiksin A., White M., 2003, *MNRAS*, 342, 1205
- Meiksin A., White M., 2004, *MNRAS*, 350, 1107
- Mesinger, A., Furlanetto, S., 2009, *MNRAS*, 400, 1461
- Pando, J., Lipa, P., Greiner, M. & Fang, L.Z., 1998, *ApJ*, 496, 9
- Paschos, P., & Norman, M. L., 2005, *ApJ*, 631, 59
- Peacock, J., 1999, *Models for Large-Scale Structure*, elss, conf, 64P
- Peebles, P. J. E. 1980, *The Large-Scale Structure of the Universe* (Princeton: Princeton Univ. Press)
- She, Z.S. & Leveque, E., 1994, *Phys. Rev. Lett.* 72, 336
- She, Z.S. & Waymire, E.C., 1995, *Phys. Rev. Lett.* 74, 262
- Songaila, A. & Cowie, L. 2002, *AJ*, 123, 2183
- Theuns, T. et al., 1998, *MNRAS*, 301, 478
- White, S.D.M. 1979, *MNRAS*, 186, 145
- Wyithe, J. & Loeb, A., 2005, *ApJ*, 625, 1
- Zhang, Y. Anninos, P., Norman, M. L., & Meiksin, A. 1997, *ApJ*, 485, 496
- Zhu, W.S., Feng, L.L. & Fang, L.Z. 2010, *ApJ*, 712, 1
- Zuo, L. 1992, *MNRAS*, 258, 36